nature climate change

ARTICLES

PUBLISHED ONLINE: 17 JULY 2017 | DOI: 10.1038/NCLIMATE3335

Localized rapid warming of West Antarctic subsurface waters by remote winds

Paul Spence[1*], Ryan M. Holmes[1,2], Andrew McC. Hogg[3], Stephen M. Griffies[4], Kial D. Stewart[3] and Matthew H. England[1]

The highest rates of Antarctic glacial ice mass loss are occurring to the west of the Antarctica Peninsula in regions where warming of subsurface continental shelf waters is also largest. However, the physical mechanisms responsible for this warming remain unknown. Here we show how localized changes in coastal winds off East Antarctica can produce significant subsurface temperature anomalies (>2 °C) around much of the continent. We demonstrate how coastal-trapped barotropic Kelvin waves communicate the wind disturbance around the Antarctic coastline. The warming is focused on the western flank of the Antarctic Peninsula because the circulation induced by the coastal-trapped waves is intensified by the steep continental slope there, and because of the presence of pre-existing warm subsurface water offshore. The adjustment to the coastal-trapped waves shoals the subsurface isotherms and brings warm deep water upwards onto the continental shelf and closer to the coast. This result demonstrates the vulnerability of the West Antarctic region to a changing climate.

The rate of global sea level rise between 1993 and 2010 is estimated to have increased by ∼150% relative to the 1901–1990 average rate[1]. The flow of grounded Antarctic glacial ice into the ocean contributed ∼28% to global sea level rise between 1960 and 2004, and its contribution is likely to increase[2]. From 2003 to 2014 the rate of West Antarctic ice mass loss has doubled[3], while from 1996 to 2013 the Totten Glacier in East Antarctica thinned by ∼12 m at the grounding line[4] (that is, the point where the ice sheet starts to float). Antarctic glacial ice loss is primarily influenced by ocean–ice interactions at the base of the floating ice shelves where basal melt rates are estimated to increase by $\sim 10\,\mathrm{m\,yr^{-1}}$ for a 1 °C increase in ocean temperatures[5,6]. The focus of this study is on the mechanisms that give rise to subsurface ocean warming around the Antarctic continental margin[7]. Future contributions from Antarctic ice sheets are the largest source of uncertainty in sea level projections because many Antarctic ice sheets are hypothesized to become rapidly unstable when warmer ocean water causes the ice sheet grounding line to retreat[8–10]. Recent estimates suggest that Antarctica could contribute >1 m of sea level rise by 2100 and >15 m by 2500[11].

Constraining Antarctica's contribution to global sea level rise requires understanding the water mass interactions across the near-circumpolar Antarctic Slope Front. This front separates the cold, fresh waters on the continental shelf from the warmer, saltier Circumpolar Deep Water generally found offshore[12]. Antarctic coastal ocean observations suggest warming of 0.1–0.3 °C per decade since 1990 on the continental shelves of the Bellingshausen Sea and Amundsen Sea and along the western side of the Antarctica Peninsula[7]. This warming is linked with a shallowing of the mid-depth temperature maximum over the continental slope and shelf that allows the warmer offshore water to flow onshore. The warming trends positively correlate with observed estimates of rapidly increasing rates of glacial ice mass loss since the 1990s[13,14].

The mechanisms responsible for the observed warming of West Antarctic continental shelf waters remain highly uncertain. Some studies suggest that a positive trend in the Southern Annular Mode (SAM), associated with strengthened and poleward shifted Southern Hemisphere mid-latitude winds[15], can aid the intrusion of warm offshore waters onto the Antarctic continental shelf. For example, *in situ* Bellingshausen Sea observations spanning the summer seasons from 1993 to 2004 highlight a large coastal intrusion of offshore subsurface waters that is correlated with a positive SAM index[16]. A mesoscale eddy-permitting ocean model also demonstrated how SAM-induced wind changes can generate subsurface Antarctic coastal warming by anomalous shallowing of isotherms[17]. Finer resolution regional and idealized ocean model studies propose that the transport of heat across the Antarctic Slope Front can also be driven by mesoscale eddies[18,19] and tides[20].

The positive SAM trend observed since the 1950s is projected to persist through the twenty-first century[21], raising concerns that it may lead to increased basal melt rates from anomalous intrusion of warm Circumpolar Deep Water onto the shelf. Prior studies have largely focused on the direct local impacts of changing winds on the Antarctic coastal ocean temperature structure[17–19]. However, observed subsurface coastal warming has been most rapid on the western side of the Antarctic Peninsula[7], despite evidence that the influence of the SAM on the coastal winds is largest in East Antarctica (Fig. 1a and Supplementary Fig. 1). Here we seek to understand why the strongest warming of Antarctic subsurface coastal waters appears west of the Antarctic Peninsula. We propose that the warming to the west of the Antarctic Peninsula can be forced by changes in remote Antarctic coastal winds.

Coastal ocean response to East Antarctic winds

Our experimental design is based on a previous study wherein a positive SAM wind perturbation applied along the entire

[1]ARC Centre of Excellence for Climate System Science and Climate Change Research Centre, University of New South Wales, Sydney, New South Wales 2052, Australia. [2]School of Mathematics and Statistics, University of New South Wales, Sydney, New South Wales 2052, Australia. [3]ARC Centre of Excellence for Climate System Science and Research School of Earth Sciences, Australian National University, Canberra, Australian Capital Territory 2601, Australia. [4]NOAA Geophysical Fluid Dynamics Laboratory, Princeton, New Jersey 08540, USA. *e-mail: paul.spence@unsw.edu.au

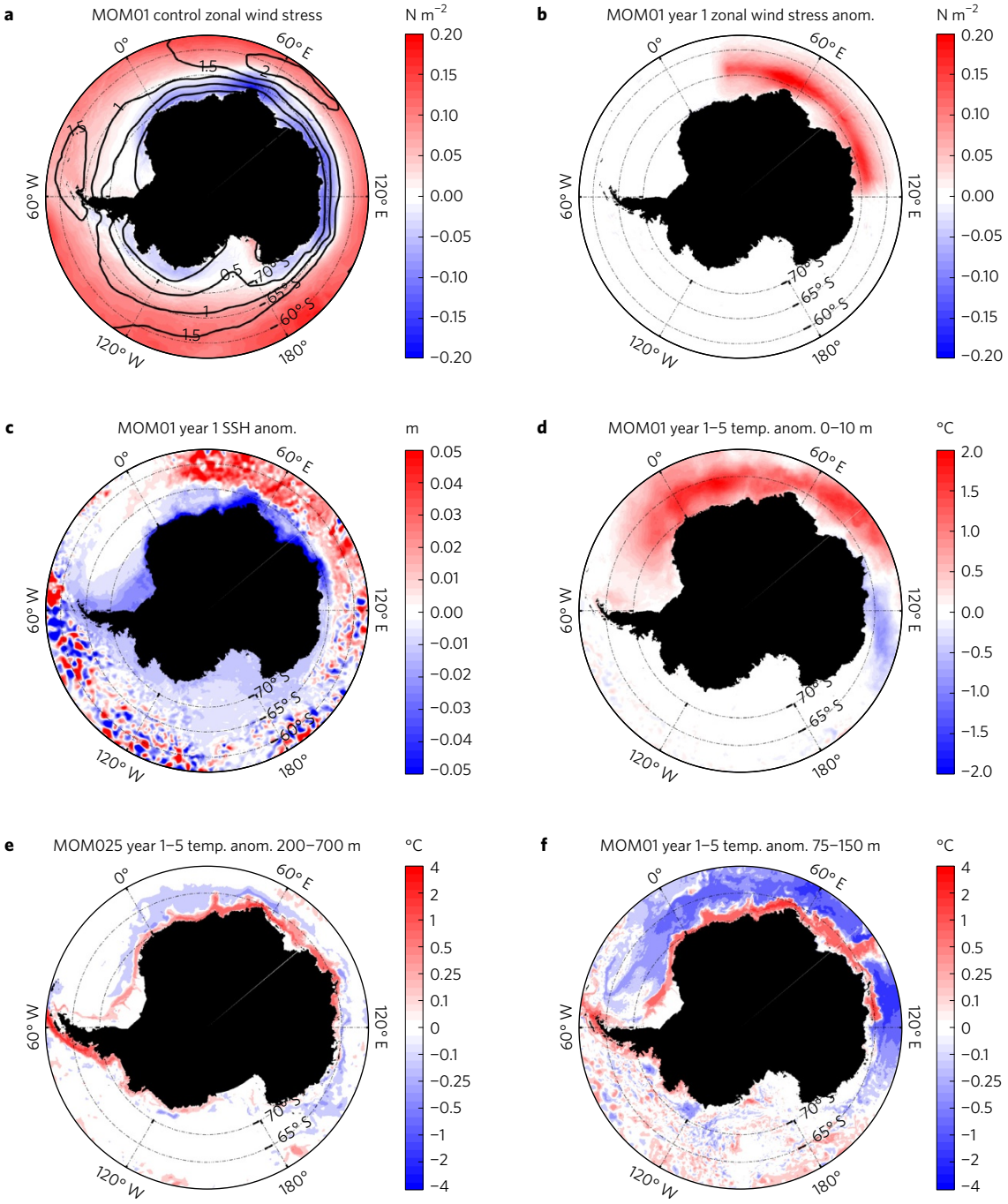

Figure 1 | Annual mean model response to East Antarctic poleward intensifying winds. a, Annual mean zonal wind stress (N m^{-2}) in the MOM01 control simulation (colours). Contour lines show zonal wind speed regression (m s^{-1}) on the non-dimensional SAM index (defined as the index minus its mean divided by its standard deviation, both mean and standard deviation being calculated considering only values prior to 1970). The SAM index is calculated by subtracting the zonal mean sea-level pressure at the latitude closest to 65° S from the zonal mean sea-level pressure at the latitude closest to 40° S. We use the CORE-II reanalysis sea-level pressure and 10 m winds over 1948–2007 for the regression[40]. **b**–**d**, Annual mean zonal wind stress anomaly (N m^{-2}) (**b**) and sea surface height anomaly (m) (**c**) in year 1 of the MOM01 wind perturbation simulation, and ocean temperature (°C) anomaly (**d**) averaged between 0 and 10 m depth in years 1–5 of the MOM01 wind perturbation simulation. Note that **a**–**d** are essentially the same for the MOM025 model. **e**, MOM025 ocean temperature (°C) anomaly averaged between 200 and 700 m depth and years 1 to 5 of the wind perturbation. **f**, MOM01 ocean temperature (°C) anomaly averaged between 75 and 150 m depth and years 1 to 5 of the wind perturbation. Note the nonlinear colour scale in **e** and **f**.

Antarctic coastline creates near-circumpolar warming (>2 °C) of the subsurface (200–700 m depth) coastal waters[17]. The warming in that study was attributed to the anomalous intrusion of warm Circumpolar Deep Water onto the shelf in response to the reduction in coastal surface Ekman pumping due to the local wind change. Here, unlike the previous study, the positive SAM wind perturbation is applied only along the East Antarctic coastline between 20° E–120° E (Fig. 1a,b; Methods). The effect of this East Antarctic wind perturbation is investigated with two global ocean sea-ice models (known as MOM01 and MOM025) that differ only in the resolution of their vertical and horizontal grids. MOM01 (MOM025) has ∼4.5 km (∼11 km) horizontal grid spacing at

65° S and 75 (50) vertical levels. The perturbation responses are qualitatively consistent between MOM025 and MOM01 in that the signs of change are robust. Quantitative differences between the two models help to constrain the forcing response and the mechanisms responsible.

The East Antarctic wind perturbation produces both local and remote impacts along the Antarctic continental margin. Firstly, it causes a circumpolar decrease in Antarctic coastal sea level that is amplified as the perturbation persists. After one year, sea level falls by ∼6 cm in the East Antarctic perturbation region, and 1–2 cm on the western side of the Antarctic Peninsula over 6,000 km away (Fig. 1c). By year 5, sea level has dropped by ∼15 cm in the wind perturbation region, and ∼10 cm west of the peninsula. In the previous study where the same wind perturbation was applied over the entire Antarctic coastline, a similar circumpolar drop in coastal sea level was attributed to a reduction in local wind-driven onshore surface Ekman transport[17]. Here, surface Ekman transport cannot explain the sea level decline found outside of the wind perturbation region.

The subsurface warms substantially around roughly 2/3 of the Antarctic coastline in both models, although at different depth ranges (Fig. 1e,f). In MOM025 intense warming occurs between 200 and 700 m depth with a maximum warming of >4 °C on the western side of the peninsula after 5 years. This response is roughly equivalent to the previous study wherein a circumpolar wind perturbation was applied in MOM025 (ref. 17). In MOM01 the warming is focused at shallower depths (75–150 m) with a maximum warming of ∼2 °C on the western side of the peninsula after 5 years. In both models, the subsurface temperature along the western coastline of the Antarctic Peninsula increases in the first year, with little other evidence of change outside of the perturbation region (Fig. 2a and Supplementary Figs 2 and 3). As the forcing persists, the subsurface warming grows in circumpolar extent and becomes intensified at the peninsula (Fig. 2b and Supplementary Figs 2 and 3). Yet the near surface ocean temperature west of the Antarctic Peninsula shows little change (cooling of <−0.1 °C; Fig. 1d) and the sea ice thickness is slightly increased (2–5 cm, not shown). There is little subsurface temperature change in the Ross Sea sector in both models (Supplementary Figs 2 and 3).

The progressive warming of shelf waters on the western side of the peninsula coincides with a shallowing of isotherms. In the unperturbed state of MOM01 the 0 °C isotherm is located at ∼125 m depth on the western shelf of the peninsula and it shoals by as much as 60 m after 5 years of the East Antarctic wind forcing (Fig. 2c,d). In MOM025 this isotherm is normally found at ∼300 m depth and it shoals by as much as 200 m with the wind perturbation. The drop in coastal sea level is accompanied by geostrophically balanced along-shelf coastal velocity anomalies directed northeastward on the western side of the peninsula and southward on the eastern side (Fig. 2e). As the wind perturbation persists, the sea level and velocity anomalies also progressively increase. After about 3 years, warming develops on the northeastern coastline of the peninsula (Fig. 2b) primarily from heat being advected eastward around the tip of the peninsula. Upward vertical velocity anomalies on the peninsula shelf (Fig. 2f) are roughly equivalent to the previous study wherein a circumpolar wind perturbation was applied.

Mechanisms for intensified subsurface warming

We now examine the physical mechanisms by which East Antarctic wind perturbations can impact Antarctic coastal ocean properties thousands of kilometres away. We begin by tracking the westward coastal propagation of anomalies from their East Antarctic source region to the Ross Sea along a coastal contour that follows the subsurface temperature anomalies on the continental shelf (Fig. 3a). A Hovmöller (distance–time) plot of temperature anomalies at 5-day intervals shows widespread subsurface coastal ocean warming along this contour line and averaged between 200 and 700 m depth in MOM025 and 75–150 m depth in MOM01 (Fig. 3b,c). The warming develops a focused intensity on the western side of the Antarctic Peninsula, 6,000 km away from the western edge of the wind perturbation. In both models, subsurface warming on the western side of the peninsula often exceeds 2 °C within 5 years.

Ensembles of both the unperturbed and wind anomaly simulations reveal the perturbation response relative to background oceanic variability (Methods). In both models, the first indications of change outside of the perturbation region are found scattered on the western side of the peninsula within the first week (not shown). A coherent warming (<0.1 °C) signature appears on the Hovmöller section near the tip of the peninsula within 50 days (Fig. 3d). After 90 days, the Antarctic Peninsula anomaly can locally exceed 0.5 °C in both models. When averaged along a section on the western side of the peninsula, the ensemble mean warming at the end of the first year exceeds one standard deviation of the control experiment variability by +0.14 °C in MOM01 (Fig. 3e) and 0.3 °C in MOM025 (not shown). It takes just 120 days for the ensemble mean warming along this section to exceed one standard deviation of the background oceanic variability in both models.

We now describe the physical mechanisms controlling the adjustment of the coastal circulation to the East Antarctic wind perturbation, and explain why the subsurface warming is most intense on the western side of the Antarctic Peninsula. The advective timescale from the perturbation region via westward coastal currents is more than two years and passive tracers released in the perturbation region never travel around the peninsula. Coastal baroclinic waves (that is, waves with structure that varies with depth) initiated by wind forcing are capable of remotely modifying the subsurface coastal density structure on faster timescales[22–24]. However, there are several strands of evidence suggesting that baroclinic waves do not make a significant contribution west of the peninsula. First, they are not resolved near Antarctica in MOM025 and are only partially resolved in MOM01 (ref. 25), even though warming is found in both models. Second, the first baroclinic gravity-wave phase speed near the Antarctic coast is <1.0 m s^{-1}, requiring >70 days for them to reach the peninsula[26]. Their influence will probably develop gradually, taking longer than the warming timescale identified in the simulations. Third, baroclinic waves may have difficulty navigating the complex coastline without substantial dissipation given their small deformation radius[27].

Westward propagating barotropic coastal Kelvin waves, in contrast, are well resolved by both models. These fast waves carry sea surface height (that is, sea level) and barotropic (that is, uniform with depth) current anomalies along the coast, but decay away from the coast over the barotropic deformation radius of ∼1,000 km. They can be generated by atmospheric forcing and are observed circumnavigating Antarctica in less than 2 days, with phase speeds of 156–192 m s^{-1} (ref. 28). The sea level signature of barotropic waves is clearly identifiable in the simulations with phase speeds that match the theoretical and observed estimates (Fig. 3f). These barotropic Kelvin waves rapidly transmit anomalies westward, driving a progressive drop in coastal sea level away from the perturbation region.

To understand the mechanisms by which sea surface height anomalies associated with the barotropic waves modify the subsurface, we now examine an area-averaged transect oriented perpendicular to the continental shelf edge on the western side of the peninsula (Fig. 4a). The Southern Ocean State Estimate[29] (SOSE) and summer time hydrographic observations[30,31] suggest that below 100 m depth the shelf water temperature in this region ranges from roughly −0.5 °C to 1 °C, and the vertical and cross-shelf density gradients are weak (Fig. 4d and Supplementary Fig. 4). In the unperturbed state of MOM025 the shelf water temperature

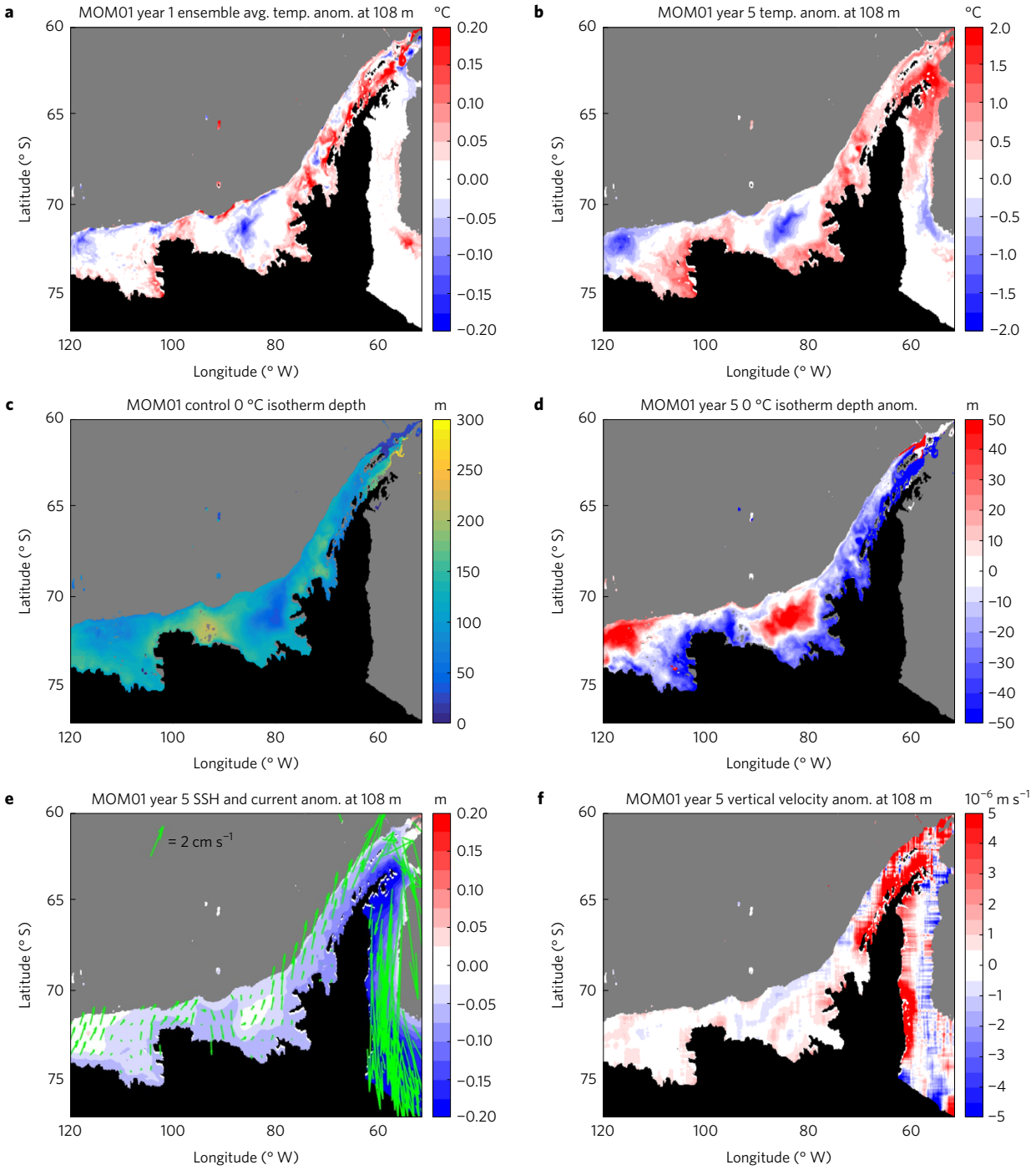

Figure 2 | Antarctic Peninsula shelf response to East Antarctic poleward intensifying winds. a, MOM01 ensemble mean temperature anomaly (°C) computed as the difference between the ten-member ensemble mean of the perturbation and control simulations over the first year at 108 m depth. **b**, MOM01 annual mean temperature anomaly (°C) at 108 m depth in the fifth year of perturbation. **c**, Depth (m) of the 0 °C isotherm in the MOM01 control state. **d**, MOM01 0 °C isotherm depth (m) anomaly in year 5. **e**, MOM01 sea surface height (colours, m) anomaly and current anomaly (vectors, cm s^{-1}) at 108 m depth in year 5 of the perturbation. The current anomaly is area-smoothed and every tenth vector is plotted. **f**, MOM01 area-smoothed vertical velocity (m s^{-1}, positive upwards) anomaly in year 5. Note regions with depths >2,000 m are shaded grey in all panels. In **c** and **d** grey shading masks both depths >1,000 m and places where the 0 °C isotherm is not found at depths <1,000 m.

below 100 m is often colder than −1 °C and there are overly strong cross-shelf and vertical density gradients (Fig. 4b) compared with observations in this region. In the unperturbed state of MOM01, the shelf waters are warmer (∼0.5 °C) and the density gradients are slightly weaker than observations suggest (Fig. 4c). The two model experiments thus span the observations and the state estimate in this regard, and thereby provide something of an upper and lower bound to the warming that can be attributed to the remote winds. The colder water and stronger density gradients at depth on the shelf lead to a relatively stronger adjustment and warming response at depth in MOM025 compared with that of MOM01.

The decrease in sea level around the coastline is mirrored by a lifting of the boundary between the cold near-surface water, and the warmer layer below (Figs 2d,e and 4e–h). This lifting occurs due to

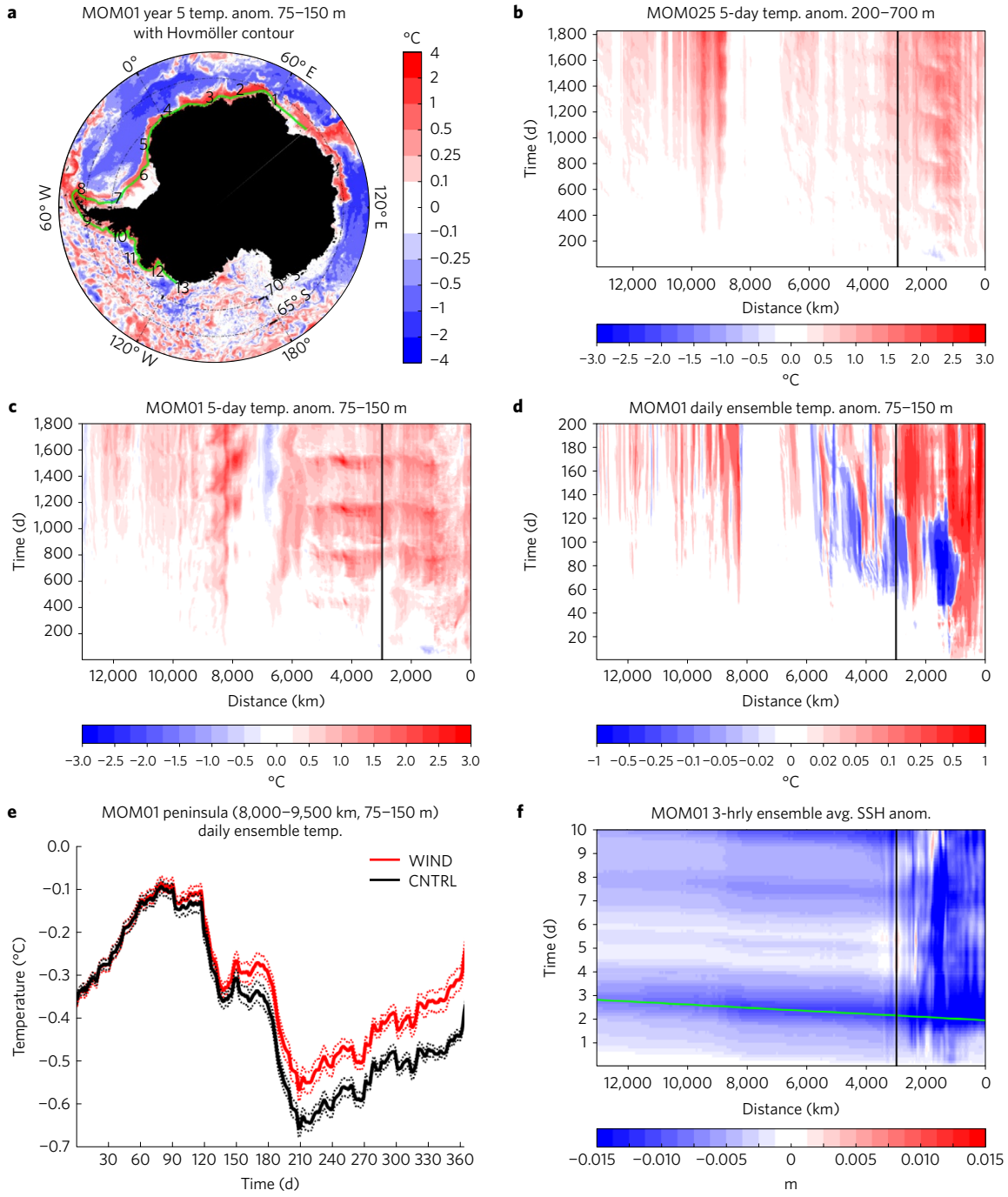

Figure 3 | Hovmöller and time-series plots of Antarctic coastal ocean response to East Antarctic poleward intensifying wind forcing. a, MOM01 annual mean ocean temperature (°C) anomaly averaged between 75 and 150 m depth in year 5 of the wind perturbation. Values in **b**–**f** are averaged over a ~3,500 km^2 area around points on the green coastal contour line in **a**. Black numbers along the green line indicate the distance along the contour in 1,000 km intervals. **b**, Hovmöller (distance–time) of 5 years of average temperature anomalies (°C) between 200 and 700 m depth at 5-day intervals in MOM025. The tip of the Antarctic Peninsula is at ~8,200 km on the *x* axis. **c**, Same as **b** except averaged 75–150 m depth in MOM01. **d**, Hovmöller of daily ensemble mean temperature anomalies (°C) computed as the difference between the ten-member ensemble mean of the perturbation and control simulations over the first year averaged between 75 and 150 m depth in MOM01. **e**, Ensemble time series of daily temperature (°C) averaged between 75 and 150 m depth and over the 8,000–9,500 km section of the coastal contour in **a**, which is located on the western side of the West Antarctic Peninsula. The solid red (black) line is the ten-member ensemble mean in wind perturbation (control) simulation. The dashed lines indicate a 1 standard deviation range among the ensemble members. **f**, Hovmöller of ensemble mean coastal sea level anomaly (m) at 30-min intervals for 60 days in MOM01. The green line in **f** indicates the theoretical prediction for the phase speed of a barotropic coastal Kelvin wave (roughly 156–192 m s^{-1}; ref. 28). The vertical black line in **b**–**d**,**f** indicates the western edge of the wind perturbation region.

baroclinic adjustment mechanisms occurring both near the seafloor and in the ocean interior on the continental shelf. In MOM025, the main adjustment to the anomalous northeastward barotropic flow develops along the continental shelf edge (Fig. 4e,g,i). The anomalous velocity signal near the shelf edge decreases towards the seafloor (Fig. 4i below 250 m), suggesting that bottom friction is

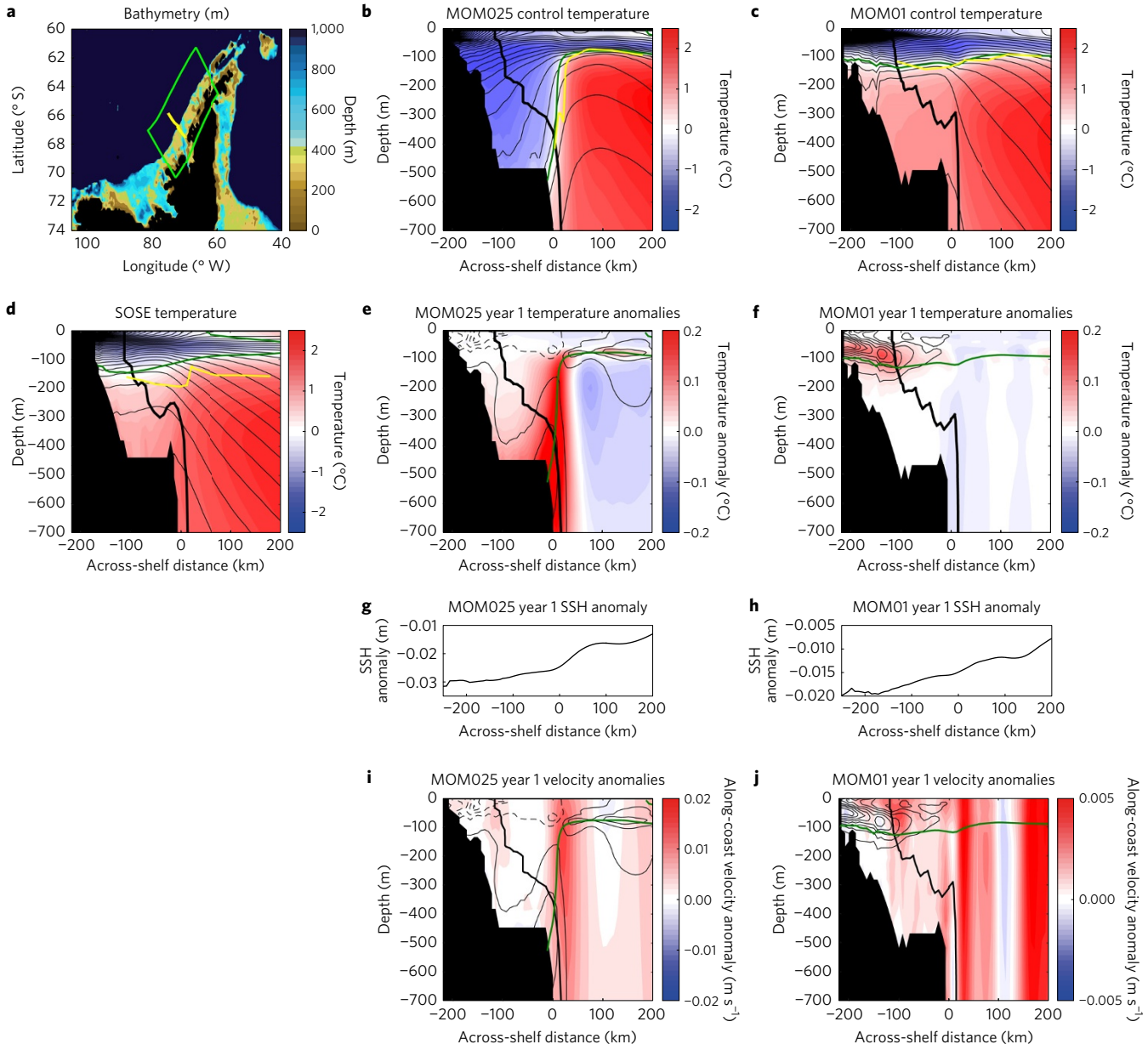

Figure 4 | Across-shelf transects of western side of peninsula response to East Antarctic wind perturbation. a, Depth of bathymetry (m) on the Antarctic Peninsula. Across-shelf-depth slices in **b–j** are averaged along the shelf within the green region in **a**. Yellow markers in **a** indicate the World Ocean Circulation Experiment line SO4P of hydrographic observations. **b**,**c**, The unperturbed state of MOM025 and MOM01 temperature (colour; the green indicates the 0 °C isotherm) and 0.1 kg m^{-3} density contours (black) averaged along the shelf within the green box in **a**. The yellow line in **b** and **c** indicates the 0 °C isotherm in the models along the SO4P line. **d**, Same as **b** except for the Southern Ocean State Estimate; the yellow line in **d** indicates the 0 °C isotherm from hydrographic observation along the SO4P line. **e**,**f**, Year 1 ensemble average temperature anomalies for MOM025 (**e**) and MOM01 (**f**), with 0.005 kg m^{-3} density anomaly contours (solid: positive; dashed: negative). **g**,**h**, Year 1 ensemble average along-shelf sea surface height anomaly for MOM025 (**g**) and MOM01 (**h**). **i**,**j**, Year 1 ensemble average along-shelf velocity anomalies for MOM025 (**i**) and MOM01 (**j**), with 0.005 kg m^{-3} density anomaly contours. Locations where less than 20% of the grid points along the section at that *x*–*z* location were within the ocean have been masked out in black, and the thick black line indicates where 90% of grid points were within the ocean.

acting. This decreased velocity anomaly then allows the anomalous onshore barotropic pressure gradient associated with the cross-shelf sea level gradient anomaly to overcome the anomalous Coriolis force, breaking the constraint of geostrophy, and driving an anomalous upslope bottom Ekman flow. The upslope flow drives a bottom intensified shallowing of bottom density surfaces and an accompanying subsurface warming (Fig. 4e). This warming also penetrates into the interior to influence a layer much thicker than the relatively thin (<30 m) Ekman layer through upward diffusion and interior baroclinic adjustment processes[32,33].

The stronger temperature gradients near the shelf break make this near-bottom isotherm shoaling mechanism more important in MOM025 than MOM01. A similar mechanism is acting in MOM01; however, it occurs closer to the coast where the density and temperature gradients are larger (Fig. 4f,h,j). The maximum temperature change occurs where the temperature gradients, including both vertical and horizontal components, are largest. For both models and the observations, these temperature gradients are largest near the 0 °C isotherm on the western side of the peninsula. The warming is deeper in MOM025 since the 0 °C

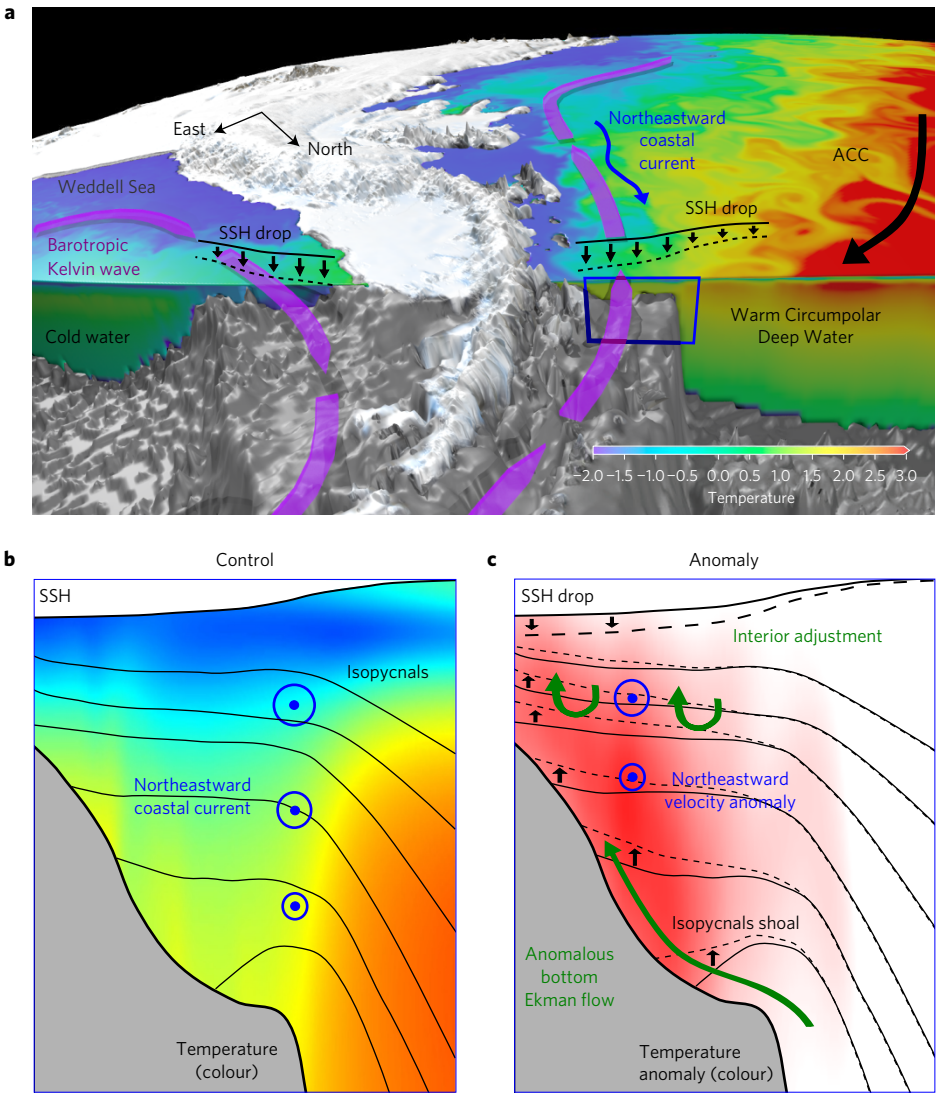

Figure 5 | Schematic of the warming response of West Antarctic Peninsula waters to East Antarctic wind perturbation. a, View of the West Antarctic Peninsula with bathymetry in grey shading, and temperature in colour. Note the warm Circumpolar Deep Water brought close to the continent by the Antarctic Circumpolar Current (ACC) on the western side. The purple arrows indicate the pathway of barotropic Kelvin waves propagating from East Antarctica. The blue box illustrates the location of across-shelf transects in **b** and **c**. **b**, Vertical, across-shelf transect on the western side of the peninsula showing the temperature structure (colour) and density surfaces (black isopycnal contours) in an unperturbed state. The low sea surface height near the coast is associated with the geostrophic northeastward coastal current (blue dots indicating flow out of the page and the surrounding circle size indicating the flow strength). **c**, Vertical, across-shelf transect on the western side of the peninsula of anomalies initiated by barotropic Kelvin waves generated by an East Antarctic wind perturbation. Barotropic Kelvin waves transmit a drop in coastal sea level along the Antarctic coastline, creating a northeastward barotropic velocity anomaly. In response, the interior isopycnals shoal through both interior baroclinic adjustment and anomalous upslope bottom Ekman flow (green arrows), allowing the velocity anomaly to decay with depth (blue arrowheads). The shoaling of isopycnals brings warm, deep water upwards and towards the coast driving subsurface warming (colour).

isotherm sits deeper on the shelf break and is more sloped than in MOM01. Hydrographic observations may clarify the depth where the maximum temperature response occurs in nature. On an observed cruise line the 0 °C isotherm sits on the peninsula shelf break at ∼200 m depth in the summertime hydrography[31] (Fig. 4a,d) and it probably deepens in winter. Along the same line the annual mean 0 °C isotherm sits on the shelf break at ∼400 m in MOM025, and ∼125 m in MOM01 (Fig. 4b,c); further evidence that the two models provide upper and lower limits to the observed thermal structure.

Both bottom and interior processes act in tandem to bring about the necessary adjustment to the barotropic wave anomaly and create warming focused around the 0 °C isotherm. While the temperature anomaly in MOM01 appears to be above the seafloor (Fig. 4f), much of it is near the seafloor (Supplementary Fig. 5) as the bathymetry varies considerably along the Fig. 4 section. Overall, these mechanisms facilitate a change of both the barotropic and baroclinic structure of the continental shelf and coastal currents without a local change in wind forcing. The same features are found in other remote locations along the Antarctic coastline. For example, in MOM01 there is a >0.5 °C warming in some parts of the Amundsen Sea and the Bellingshausen Sea within five years (Figs 1 and 2).

We conclude that the warming is largest on the western side of the Antarctic Peninsula region for two main reasons. Firstly, the interior temperature gradients are large on the western side of the peninsula due to the close proximity to warm, salty water advected close to the continental shelf by the Antarctic Circumpolar Current

(Fig. 4b–d and Supplementary Fig. 4). The presence of this warm, salty Circumpolar Deep Water allows the anomalous flow to create a stronger warming signal in this region. Secondly, we suggest that the anomalous cross-shelf sea level gradients and velocity anomalies are large there due, at least in part, to topographic steering by the particularly steep shelf edge bathymetry (Supplementary Fig. 6). The depth-integrated geostrophic velocity is constrained to follow contours of constant f/h, where f is the Coriolis parameter and h is the water depth. Consequently, the along-shelf velocity anomalies are strongest along regions of the Antarctic coastline, including the western side of the Antarctic Peninsula, that are characterized by a steep continental slope (Supplementary Fig. 6a). This region is well connected to the East Antarctic wind perturbation region via f/h contours and the barotropic circulation there responds to changes in winds around the entire Antarctic coastline[34]. The timescale and spatial distribution of the velocity created by the East Antarctic wind perturbation is well reproduced in a single-layer shallow-water model, which predicts a particularly strong anomalous barotropic flow along the shelf and shelf break on the western side of the peninsula (Methods, Supplementary Fig. 6d). The mechanism proposed here predicts the largest onshore transport in regions with the largest alongshore barotropic velocity anomaly.

Summary

Figure 5 presents a schematic that summarizes the physical mechanisms whereby barotropic waves forced by a remote Antarctic coastal wind perturbation can rapidly produce intense warming of the subsurface Antarctic coastal ocean with a focused intensity on the western side of the Antarctic Peninsula. First, a reduction in polar easterlies gradually decreases the local East Antarctic coastal sea level as anomalous surface Ekman transport pumps water offshore. This drop in sea level is then propagated around the Antarctic coastline by a barotropic Kelvin wave. Next, the sea level drop creates a cross-shelf sea level gradient anomaly and an along-shelf geostrophically balanced horizontal velocity anomaly, which is particularly strong on the western side of the Peninsula. Due to both bottom-boundary layer friction and interior adjustment, this horizontal velocity anomaly decreases in the warm, less stratified waters below the thermocline. To maintain geostrophic balance, this anomalous vertical shear is accompanied by a shoaling of the subsurface density layers close to the coast. This shoaling then facilitates the movement of warmer deep water upward onto the continental shelf and toward the coast.

A reduction in surface Ekman pumping by a local coastal wind perturbation also creates warming on the shelf[17], as found in the East Antarctic perturbation region in this study. However, here we show that the influence of remote winds on the subsurface coastal ocean can be just as large as that of the local winds. The observed subsurface warming rates on the western side of the peninsula, and in the Amundsen and Bellingshausen seas are estimated at $\sim$0.5 °C since 1990[7]. The remote wind perturbation response presented here can create this magnitude of warming in less than a decade. The remote wind perturbation considered here was motivated by the projected influence of the SAM on East Antarctic coastal winds. However, Antarctic coastal wind disturbances are not unique to the SAM or East Antarctica. Well-documented links between other climate modes of variability and Antarctic coastal winds can produce a similar barotropic coastal ocean response[26,35,36].

Accurately modelling observed features of the Antarctic coastal environment requires very fine resolution models. In particular, the inclusion of katabatic winds[37], ice cavity interactions[38,39], tides[20] and mesoscale ocean eddies[18,19] in the Antarctic coastal region requires horizontal grids finer than 1 km. Eddy-driven processes[18,19] and tidal influences[20] certainly play a role in the equilibrium heat budget on the continental shelf, but it is difficult to predict significant changes to them. At finer resolution a more vigorous mesoscale eddy field could further enhance cross-shelf exchange of warm water. Observations also suggest that Antarctic Circumpolar Current filaments impinging on the shelf break can generate onshore flows in topographic channels via bottom Ekman dynamics similar to those presented here[33]. Remotely generated sea level anomalies may drive a portion of these topographic channel intrusions. Currently there is no theoretical framework or numerical model that can simultaneously represent all of the relevant processes, making quantitative comparisons between the relevant mechanisms difficult.

We have documented the sensitivity of the Antarctic coastal ocean to remote atmospheric wind perturbations, particularly ocean properties on the western side of the Antarctic Peninsula. This sensitivity is due to a conspiracy between the proximity of the relatively warm Circumpolar Deep Water and the steep shelf bathymetry in the region, with circumpolar impacts facilitated by coastal-trapped barotropic waves. This mechanism helps explain the vulnerability of the West Antarctic marine grounded ice sheets to subsurface ocean warming, with potentially profound implications for global sea level rise over the coming decades.

Methods

Methods, including statements of data availability and any associated accession codes and references, are available in the online version of this paper.

Received 25 January 2017; accepted 8 June 2017; published online 17 July 2017

References

1. Hay, C., Morrow, E., Kopp, R. & Mitrovica, J. Probabilistic reanalysis of twentieth-century sea-level rise. *Nature* **517,** 481–484 (2015).
2. Hock, R., de Woul, M., Radic, V. & Dyurgerov, M. Mountain glaciers and ice caps around Antarctica make a large sea-level rise contribution. *Geophys. Res. Lett.* **36,** L07501 (2009).
3. Harig, C. & Simon, F. Accelerated West Antarctic ice mass loss continues to outpace Antarctic gains. *Earth Planet. Sci. Lett.* **415,** 134–141 (2015).
4. Li, X., Rignot, E., Morlighem, M., Mouginot, J. & Scheuchl, B. Grounding line retreat of Totten Glacier East Antarctica. 1996–2013. *Geophys. Res. Lett.* **42,** 8049–8056 (2015).
5. Rignot, E. & Jacobs, S. Rapid bottom melting widespread near Antarctic ice sheet grounding lines. *Science* **296,** 2020–2023 (2002).
6. Rignot, E., Jacobs, S., Mouginot, J. & Scheule, B. Ice-shelf melting around Antarctica. *Science* **341,** 266–270 (2013).
7. Schmidtko, S., Heywood, K., Thompson, A. & Aoki, S. Multidecadal warming of Antarctic waters. *Science* **346,** 1227–1231 (2014).
8. Church, J. A. *et al*. *Climate Change 2013: The Physical Science Basis* (eds Stocker, T. F. *et al*.) Ch. 13 (IPCC, Cambridge Univ. Press, 2013).
9. Joughin, I., Smith, B. E. & Medley, B. Marine ice sheet collapse potentially under way for the Thwaites Glacier Basin. West Antarctica. *Science* **344,** 735–738 (2014).
10. Favier, L. *et al*. Retreat of Pine Island Glacier controlled by marine ice-sheet instability. *Nat. Clim. Change* **4,** 117–121 (2014).
11. DeConto, R. & Pollard, D. Contribution of Antarctica to past and future sea-level rise. *Nature* **531,** 591–597 (2016).
12. Jacobs, S. S. On the nature and significance of the Antarctic Slope Front. *Mar. Chem.* **35,** 9–24 (1991).
13. Rignot, E. *et al*. Recent Antarctic ice mass loss from radar interferometry and regional climate modeling. *Nat. Geosci.* **1,** 106–110 (2008).
14. Cook, A. *et al*. Ocean forcing of glacier retreat in the western Antarctic Peninsula. *Science* **353,** 283–285 (2016).
15. Thompson, D. W. & Solomon, S. Interpretation of recent Southern Hemisphere climate change. *Science* **296,** 895–899 (2002).
16. Martinson, D., Stammerjohn, S., Iannuzzi, R., Smith, R. & Vernet, M. Western Antarctic Peninsula physical oceanography and spatio-temporal variability. *Deep-Sea Res. II* **55,** 1964–1987 (2008).
17. Spence, P. *et al*. Rapid subsurface warming and circulation changes of Antarctic coastal waters by poleward shifting winds. *Geophys. Res. Lett.* **41,** 4601–4610 (2014).
18. Nøst, O. A. *et al*. Eddy overturning of the Antarctic Slope Front controls glacial melting in the Eastern Weddell Sea. *J. Geophys. Res.* **116,** C11014 (2011).

19. Stewart, A. & Thompson, A. Connecting Antarctic cross-slope exchange with Southern Ocean overturning. *J. Phys. Oceanogr.* **43,** 1453–1471 (2013).
20. Flexas, M. *et al*. Role of tides on the formation of the Antarctic Slope Front at the Weddell-Scotia Confluence. *J. Geophys. Res.* **120,** 3658–3680 (2015).
21. Zheng, F., Li, J., Clark, R. & Nnamchi, H. Simulation and projection of the Southern Hemisphere Annular Mode in CMIP5 models. *J. Clim.* **26,** 9860–9879 (2013).
22. Rhines, P. B. Edge-, bottom-, and Rossby waves in a rotating stratified fluid. *Geophys. Fluid Dyn.* **1,** 273–302 (1970).
23. Rhines, P. & Bretherton, F. Topographic Rossby waves in a rough-bottomed ocean. *J. Fluid Mech.* **61,** 583–607 (1973).
24. Wang, D. & Mooers, C. Coastal-trapped waves in a continuously stratified ocean. *J. Phys. Oceanogr.* **6,** 853–856 (1976).
25. Hallberg, R. Using a resolution function to regulate parameterizations of oceanic mesoscale eddy effects. *Ocean Modell.* **72,** 92–103 (2013).
26. Chelton, D. *et al*. Geographical variability of the first baroclinic Rossby radius of deformation. *J. Phys. Oceanogr.* **28,** 433–460 (1998).
27. Schwab, D. J. & Beletsky, D. Propagation of Kelvin waves along irregular coastlines in finite-difference models. *Adv. Water Resour.* **22,** 239–245 (1998).
28. Kusahara, K. & Ohshima, K. Kelvin waves around Antarctica. *J. Phys. Oceanogr.* **44,** 2909–2920 (2014).
29. Mazloff, M. R., Heimbach, P. & Wunsch, C. An eddy-permitting Southern Ocean state estimate. *J. Phys. Oceanogr.* **40,** 880–899 (2010).
30. Moffat, C., Owens, B. & Beardsley, R. On the characteristics of Circumpolar Deep Water intrusions to the west Antarctic Peninsula shelf. *J. Geophys. Res.* **114,** C05017 (2009).
31. Chipman, D. W. *et al*. *Carbon Dioxide, Hydrographic, and Chemical Data Obtained During the R/V Akademik Ioffe Cruise in the South Pacific Ocean* (Oak Ridge National Laboratory, US Department of Energy, 1997); http://dx.doi.org/10.3334/CDIAC/otg.ndp063
32. MacCready, P. & Rhines, P. B. Buoyant inhibition of Ekman transport on a slope and its effect on stratified spin-up. *J. Fluid Mech.* **223,** 631–666 (1991).
33. Wåhlin, A. *et al*. Some implications of Ekman layer dynamics for cross-shelf exchange in the Amundsen Sea. *J. Phys. Oceanogr.* **42,** 1461–1474 (2012).
34. Hughes, *et al*. Wind-driven transport fluctuations through Drake Passage: a southern mode. *J. Phys. Ocean.* **29,** 1971–1992 (1999).
35. Karoly, D. J. Southern hemisphere circulation features associated with El Niño-Southern Oscillation events. *J. Clim.* **2,** 1239–1252 (1989).
36. Jenkins, *et al*. Decadal ocean forcing and Antarctic Ice Sheet response: lessons from the Amundsen Sea. *Oceanography* **29,** 106–117 (2016).
37. Mathiot, P. *et al*. Sensitivity of coastal polynyas and high salinity shelf water production in the Ross Sea, Antarctica, to the atmospheric forcing. *Ocean Dynam.* **62,** 701–723 (2012).
38. Dinniman, S., Klinck, J. & Smith, W. A model study of Circumpolar Deep Water on the West Antarctic Peninsula and Ross Sea continental shelves. *Deep-Sea Res. II* **58,** 1508–1523 (2011).
39. Hellmer, H. H., Kauker, F., Timmermann, R., Determann, J. & Rae, J. Twenty-first-century warming of a large Antarctic ice-shelf cavity by a redirected coastal current. *Nature* **485,** 225–228 (2012).
40. Large, W. G. & Yeager, S. The global climatology of an inter-annually varying air-sea flux data set. *Clim. Dynam.* **33,** 341–364 (2009).

Acknowledgements

This research was undertaken on the National Computational Infrastructure (NCI) in Canberra, Australia, which is supported by the Australian Commonwealth Government. Thanks to S. Ramsden and the NCI Vizlab for helping with the schematic in Fig. 5. Thanks to NOAA/GFDL for helping with model developments. Thanks to N. Jourdain for providing Supplementary Fig. 1 and helpful comments. Thanks to E. Bergkamp for investigating baroclinic modes in idealized simulations and to O. Saenko, J. Le Sommer, A. Stewart, J. Fyke, R. Hallberg, C. Dufour, G. Marques and P. Goddard for helpful comments. P.S. was supported by an Australian Research Council (ARC) DECRA Fellowship DE150100223, A.M.H. by an ARC Future Fellowship FT120100842 and M.H.E. by an ARC Laureate Fellowship FL100100214 and R.M.H. by an ARC Discovery Project DP150101331.

Author contributions

P.S. conceived the study, conducted the global ocean modelling and wrote the initial draft of the paper. R.M.H. performed the single-layer, shallow-water modelling. P.S. and R.M.H. analysed the model data. All authors contributed to interpreting the results, discussion of the associated dynamics, and refinement of the paper.

Additional information

Supplementary information is available in the online version of the paper. Reprints and permissions information is available online at www.nature.com/reprints. Publisher's note: Springer Nature remains neutral with regard to jurisdictional claims in published maps and institutional affiliations. Correspondence and requests for materials should be addressed to P.S.

Competing financial interests

The authors declare no competing financial interests.

Methods

The global ocean sea-ice model. This study primarily uses two global ocean sea-ice models referred to as MOM025 and MOM01 that differ only in the resolution of their vertical and horizontal grids. MOM025 is the same model configuration as used in ref. 17 and has a 1/4° Mercator horizontal resolution with ~11 km grid spacing at 65° S and 50 vertical levels. MOM01 has a 1/10° Mercator horizontal resolution with ~4.5 km grid spacing at 65° S and 75 vertical levels. The Antarctic Slope Front and Antarctic coastal currents have observed horizontal widths of ~50 km, except in regions of particularly steep bathymetry (for example, Ross Sea) where the observed horizontal scale is reduced to ~20 km (refs 12,41,42). Sea surface salinity is restored to seasonally varying climatology on a 60-day timescale with a piston velocity of 0.16 m d^{-1}. The atmospheric state is prescribed and converted to ocean surface fluxes by bulk formulae, and consequently the model does not resolve air–sea feedbacks. The atmospheric forcing is derived from version 2 of the Coordinated Ocean-ice Reference Experiments Normal Year Forcing (CORE-NYF) reanalysis data[40]. CORE-NYF provides a climatological mean atmospheric state estimate at 6-hour intervals and roughly 2-degree horizontal resolution, along with representative synoptic variability. The 1/4° and 1/10° models are based on the GFDL CM2.5 and GFDL CM2.6 coupled climate models[43,44] respectively.

The models do not have ice shelf cavities and their horizontal resolution is insufficient to adequately resolve the first baroclinic Rossby radius of deformation on the Antarctic continental shelf, which requires horizontal grids finer than 1/36° Mercator resolution (<1 km; ref. 25). However, comparisons between the MOM01 and MOM025 simulations allow an understanding of the sensitivity of the results to the presence of a more vigorous eddy field as the horizontal grid is refined from 1/4° to 1/10° Mercator resolution and the vertical resolution is increased from 50 to 75 vertical levels. In particular, we note that increasing the vertical resolution greatly enhances the barotropic and baroclinic eddy kinetic energies on and surrounding the Antarctic continental shelf and slope[45].

Control state simulations. Idealized Antarctic coastal wind perturbation experiments are initiated in the 1/4° and 1/10° models from 200-year- and 50-year-long control state simulations that are forced by repeated CORE-NYF atmospheric state. The control state water mass properties are evaluated on the western side of the peninsula by comparing with the 1/6° Mercator resolution and 46 vertical level Southern Ocean State Estimate (SOSE)[29] and the World Ocean Circulation Experiment (WOCE) line SO4P of hydrographic observations[31]. For the SOSE comparison across-shelf-depth slices averaged along a large portion of the peninsula are used (Fig. 4). The continental shelf waters in this section are >1 °C colder in MOM025 and >0.5 °C warmer in MOM01 than in SOSE. Similarly, the sloped isopycnals on the continental shelf are steeper in MOM025 and flatter in MOM01 than in SOSE. When averaged between 100 m and 500 m depth within 50 km of the continental shelf edge the across-shelf temperature gradient is 0.82 °C/100 km in SOSE, 2.80 °C/100 km in MOM025 and 0.68 °C/100 km in MOM01. When evaluated along the WOCE SO4P line, the models exhibit similar temperature biases (Supplementary Fig. 4). The continental shelf waters are often >1 °C colder in MOM025 and >0.5 °C warmer in MOM01 than in the WOCE SO4P data. The 0 °C isotherm that characterizes the simulated warming response crosses the shelf break on the SO4P line at a depth of ~200 m in WOCE, ~100 m in SOSE, ~400 m in MOM025 and ~125 m in MOM01. Hence, the water mass structures in MOM01 and MOM025 straddle the observations, and thus may provide a range for the temperature response.

Wind perturbation experiments. The primary wind perturbation scenario used in this study is based on the $W_{4°S+15\%\ (62°S-70°S)}$ scenario of ref. 17, wherein the CORE-NYF 10 m winds at all longitudes between 62° S and 70° S are shifted four degrees south and increased in magnitude by 15%. This perturbation scenario was guided by an assessment of the late twenty-first-century change in Southern Ocean zonal winds in 32 climate models from the Fifth Coupled Model Intercomparison Project (CMIP5). The only difference between the $W_{4°S+15\%\ (62°S-70°S)}$ scenario of ref. 17 and the experiment considered here is that the wind perturbation is applied exclusively along the East Antarctic coastline between 20° E and 120° E (Fig. 1a,b). The wind perturbation scenario is motivated by the Antarctic polar easterly winds and their SAM regression being strongest along the East Antarctic coastline in both the CMIP5 multi-model ensemble and the CORE 1948–2007 reanalysis data (Fig. 1a, see also Supplementary Fig. 1). The wind forcing perturbation is applied as a constant anomaly to the CORE-NYF atmospheric state. Both meridional and zonal wind components are modified and smoothing is applied along the wind perturbation boundaries. Several other Antarctic wind perturbation scenarios were tested, and in all cases the ocean response was robust and roughly a linear function of the wind perturbation scenario. For example, the ocean response takes longer to manifest on the peninsula when the perturbation is ramped over time or applied further eastward, and it is weaker when the wind perturbation area is reduced.

All anomalies presented here are determined as the difference between the wind perturbation simulation and the concomitantly extended control simulation, with this approach acting to approximately remove the effects of model drift. The model results were validated with ten-member ensembles of both the control and perturbed experiments to identify the role of internal variability in the perturbation response. The ensembles are not necessary to clearly identify the perturbation response, and thus anomalies are often presented as the difference between a single control and perturbed experiment member. However, at timescales <=1 year, we choose to show an ensemble average anomaly based on daily averages to clarify the wind response. Separately averaging the ten members of each ensemble, and then taking their difference determines the ensemble average anomaly.

Single-layer shallow-water ocean model experiments. To examine the dynamics of barotropic coastally trapped waves, a single-layer ocean simulation was considered with similar forcing as the localized wind perturbation experiment considered here. For this purpose, we used the Regional Ocean Modelling System[46] (ROMS) in a linear, single-layer shallow-water configuration with a similar grid and bathymetry to MOM025, yet restricted to the region south of 30° S (where a radiation boundary condition was used). The simulation was initialized from rest, and forced with the temporally constant zonal wind stress anomaly applied in the perturbation simulation of the global ocean sea-ice models (that is, Fig. 1b) and run for 20 days with quadratic bottom drag.

Data availability. The Southern Ocean State Estimate data that support this study are publicly available at http://sose.ucsd.edu/sose_stateestimation_data_05to10.html. The World Ocean Circulation Experiment line SO4P hydrographic observations are publicly available at https://www.nodc.noaa.gov/woce/wdiu/. All MOM025, MOM01 and ROMS model simulation data are available from the corresponding author upon reasonable request.

References

41. Dong, J., Speer, K. & Jullion, L. The Antarctic slope current near 30° E. *Geophys. Res. Lett.* **121,** 1051–1062 (2016).
42. Chavanne, C. P., Heywood, K., Nicholls, K. & Fer, I. Observations of the Antarctic Slope Undercurrent in the southeastern Weddell Sea. *Geophys. Res. Lett.* **37,** L13601 (2010).
43. Griffies, S. M. *et al*. Impacts on ocean heat from transient mesoscale eddies in a hierarchy of climate models. *J. Clim.* **28,** 952–977 (2015).
44. Delworth, T. L. *et al*. Simulated climate and climate change in the GFDL CM2.5 high-resolution coupled climate model. *J. Clim.* **25,** 2755–2781 (2012).
45. Stewart, K. *et al*. Vertical resolution of baroclinic modes in global ocean models. *Ocean Model.* **113,** 50–65 (2017).
46. Shchepetkin, A. & McWilliams, J. The regional oceanic modeling system (ROMS): a split-explicit, free surface, topography following-coordinate oceanic model. *Ocean Model.* **9,** 347–401.